Journal of Adhesion Science and Technology

Structural, thermo-mechanical and morphological properties of composites made with poly(lactic acid) and poly(ethylene terephthalate) fibers without compatibilizer

--Manuscript Draft--

Manuscript Number:	JAST-2021-00439R1
Full Title:	Structural, thermo-mechanical and morphological properties of composites made with poly(lactic acid) and poly(ethylene terephthalate) fibers without compatibilizer
Short Title:	Properties of PLA/PET fiber composites
Article Type:	Research Article
Keywords:	Poly(lactic acid); Poly(ethylene terephthalate) fiber; Polymer composite; Adhesion; Contact angle; Thermal stability
Corresponding Author:	Imane MAYOUF Universite Ferhat Abbas Setif 1 Departement Genie des Procedes Sétif, -- Select a State (only if United States or Canada Algeria
Corresponding Author Secondary Information:	
Corresponding Author's Institution:	Universite Ferhat Abbas Setif 1 Departement Genie des Procedes
Corresponding Author's Secondary Institution:	
First Author:	Imane MAYOUF
First Author Secondary Information:	
Order of Authors:	Imane MAYOUF
	Melia GUESSOUM
	Zahir RAHEM
	Mónica FUENSANTA
	José Miguel MARTIN-MARTINEZ
Order of Authors Secondary Information:	
Abstract:	In this study, physical and electrostatic interactions existing between poly(lactic acid) (PLA) and poly(ethylene terephthalate) (PET) fiber were proved as a promising strategy for preparing novel lightweight PLA/PET fiber composites, without the need of adding compatibilizer or carrying out chemical/physical treatments to the fiber. The impact resistance of the PLA/PET fiber composites increased notably by adding up to 1.5 phr PET fibers thanks to the better dispersion of PET fibers and good polymer-fiber adhesion caused by the creation of hydrogen bonds between the surface hydroxyl and carbonyl groups on both polymers. However, the composites with 2-3 phr PET fibers were brittle due to PET fibers aggregation. The glass transition temperature of PLA increased moderately due to the good matrix/filler interfacial adhesion via hydrogen bond interactions, and its crystallinity showed a trivial variation contrary to the crystallites size, this decreased noticeably because of the fibers inhibiting effect. Finally, an increased thermal stability of the PLA/PET fiber composites was demonstrated.
Opposed Reviewers:	
Response to Reviewers:	

Structural, thermo-mechanical and morphological properties of composites made with poly(lactic acid) and poly(ethylene terephthalate) fibers without compatibilizer

Imane MAYOUF[1*], Melia GUESSOUM[1], Zahir RAHEM[2], Mónica FUENSANTA[3], José Miguel MARTIN-MARTINEZ[3]

[1] Laboratoire de Physico-Chimie des Hauts Polymères (LPCHP), Département de Génie des Procédés, Faculté de Technologie, Université Ferhat ABBAS Sétif-1, Sétif, 19000, Algérie

[2] Laboratoire des Matériaux Polymériques Multiphasiques (LMPMP), Département de Génie des Procédés, Faculté de Technologie, Université Ferhat ABBAS Sétif-1, Sétif, 19000, Algérie

[3] Adhesion and Adhesives Laboratory, University of Alicante, 03080 Alicante, Spain

[*] **Corresponding author: imen_myo@yahoo.fr**

Structural, thermo-mechanical and morphological properties of composites made with poly(lactic acid) and poly(ethylene terephthalate) fibers without compatibilizer

Abstract

In this study, physical and electrostatic interactions existing between poly(lactic acid) (PLA) and poly(ethylene terephthalate) (PET) fiber were proved as a promising strategy for preparing novel lightweight PLA/PET fiber composites, without the need of adding compatibilizer or carrying out chemical/physical treatments to the fiber. The impact resistance of the PLA/PET fiber composites increased notably by adding up to 1.5 phr PET fibers thanks to the better dispersion of PET fibers and good polymer-fiber adhesion caused by the creation of hydrogen bonds between the surface hydroxyl and carbonyl groups on both polymers. However, the composites with 2-3 phr PET fibers were brittle due to PET fibers aggregation. The glass transition temperature of PLA increased moderately due to the good matrix/filler interfacial adhesion via hydrogen bond interactions, and its crystallinity showed a trivial variation contrary to the crystallites size, this decreased noticeably because of the fibers inhibiting effect. Finally, an increased thermal stability of the PLA/PET fiber composites was demonstrated.

Keywords: Poly(lactic acid), Poly(ethylene terephthalate) fiber, Polymer composite, Adhesion, Contact angle, Thermal stability.

1. Introduction

There is a need in developing eco-friendly composites with high performance for complying with circular economy targets in the automotive, construction and packaging industries, and their manufacturing cost should be reduced [1-3]. To respond to these demands, in the last couple of decades, biocomposites based on thermoplastics with natural reinforcements and with 90 wt.% biodegradable content have become promising materials. These materials respect the environmental concerns and, at the same time, respond the industrial and economical challenges [2, 4-6].

Apart from agropolymer matrices, biopolyesters such as poly (lactic acid) (PLA) are the main studied/used biopolymers in biocomposites [2, 5]. Regardless to its biodegradability and biocompatibility, PLA has a relatively high elastic modulus, good processability and a chemical structure that allow simple modifications. These advantages make PLA as an adequate candidate to replace conventional petrochemical polymers [7-9]. However, the high-cost of PLA compared to commodity thermoplastics, in addition to its brittleness and reduced stiffness, still the major drawbacks that limit its extensive application particularly in the packaging of medical devices [9-13]. PLA has been vastly investigated as matrix for biocomposites and recent efforts are made in broading its usability by addition of various fillers and fibers [5, 9, 12, 14-18].

Thanks to their high mechanical strength combined with low weight and low cost, different fibers are being successfully used to reinforce polymer matrices. The aspect ratio of the fiber and its good dispersion into the polymer matrix are among the most important parameters that must be considered to obtain a composite with improved properties, the short fibers are preferred generally [9]. Furthermore, an adequate matrix-fiber interface is crucial, this is related to the interactions between the fiber surface and the matrix [19].

Both synthetic and natural fibers have been added to improve the PLA properties [15]. Samouh et al. [20] have prepared PLA/sisal fiber biocomposites and found that the dynamic mechanical properties of PLA were notably improved and its crystallinity increased to 61% by adding10 wt. % sisal fiber. Identically, Rahem et al. [12] mixed PLA with three ratios of Luffa fiber and reported an increase of the resilience due to a better interfacial adhesion in presence of maleic anhydride grafted-poly(lactic acid) (PLA-g-MA)compatibilizer. Nanthananon et al. [21] investigated PLA/eucalyptus short fiber composites in presence of three types of compatibilizers containing anhydride and epoxide groups and evidenced the interfacial reaction between PLA and eucalyptus fiber via epoxide-based reactive agent and improved fiber-matrix

adhesion. Similarly, Yu et al. [8] reported the efficiency of three types of diisocyanates as compatibilizers for PLA/ramie fiber biocomposites through SEM observations and mechanical analysis.

On the other side, synthetic fibers gained interest in biocomposites thanks to their good resistance to heat and moisture that confers a relatively better dimensional stability compared to natural fibers, thus resulting on higher composites performances especially in medical applications [9]. Wang et al. [16] added short glass fiber (GF) (4mm) modified with 3-aminopropyl methyldimethoxysilane to improve the interactions with PLA matrix; the addition of 20 wt.% GF increased the tensile strength by 46% and the elastic modulus by 60.8 %, while the elongation at break was merely sacrificed by 21.1%. Also, Wang et al. [22] reported that the addition of modified GF affected the glass transition temperature and enhanced both the thermal stability and the heat deflection temperature of PLA. Xiu et al. [23] obtained PLA/carbon fibers (CF) composites (80/20) wt.% with a good stiffness/toughness balance after adding different amounts of poly (ether) urethane as bonding agent between PLA and the carbon fibers. CF contributed in increasing the impact strength from 3.1 to 5.6 kJ/m² and the yield strength from 68.36 to 99.97 MPa. Lin et al. [24] combined both carbon and glass fibers in a PLA matrix and noticed that on increasing CF content a greater strength was attained, while GF provided a higher modulus. Additionally, Hsieh et al. [25] found that maleic anhydride grafted-styrene-ethylene-butylene-styrene (SEBS-g-MA) block copolymer improved the adhesion at the PLA/CF interface, and enhanced toughness and impact resistance of the composites were obtained.

Poly(ethylene terephthalate) (PET) fiber is one of the most used synthetic fibers, because it is tough, is made from a cheap and available polymer, and presents a low density combined to high temperature resistance and modulus. Moreover, PET fiber could be easily modified for specific applications including textile and building industry [26-29].

In order to get a concomitant advantage of both the biodegradability of the aliphatic biopolyesters and the excellent properties of the aromatic polyesters, some authors have explored the interactions between PLA and PET [10, 30-34]. The chemical affinity between the two polymers is provided by interactions between the polar carboxyl and hydroxyl groups on the polymer surfaces, which are responsible for their miscibility [30-32, 34, 35]. Interactions between PLA and PET via transesterification reaction [31], or secondary interactions by hydrogen bonding or via electrostatic forces have been reported [33, 34]. Dehas et al. [36] took advantage of such interactions and pointed out the efficiency of recycled PET fiber (rPET) in

the reinforcement of unsaturated polyester resin (UPR), and the manufacture of lightweight composites. The better mechanical properties and thermal stability were obtained for composites filled with 5-8 phr rPET fibers with lengths lower than 5 mm. The modifications in PET filled UPR matrix were significant and led us to add PET fibers to PLA for overcoming its brittleness and limited thermal resistance. To the best of our knowledge, no previous study has been published assessing the properties of PLA/PET fiber composites, and, in this paper, new PLA-based composites filled with different amounts of virgin PET fibers presenting an average length of 2-3 mm were prepared and their structural, morphological and thermo-mechanical properties were studied. The electrostatic and physical interactions produced between PLA and PET fiber would increase the interfacial adhesion without the need of chemical/physical treatment of the fiber or the addition of compatibilizers.

2. Experimental

2.1. Materials

Biodegradable thermoplastic PLA derived from vegetal resources (PLI 005) with melt flow index (MFI) (at 190°C and under 2.16 kg) of 10-30 g/10 min was supplied by Nature Plast (Caen, France). PET fiber has been fabricated in the Université Ferhat ABBAS Sétif-1 by melting virgin PET pellets (dried at 100°C for 24 hours) in a melt flow indexer (Controlab, model 5-Gennevilliers, France) at 260°C and under a load of 0.5 kg. After melting, a PET cord is extruded through a die of diameter less than 0.1mm, and then it is fixed to a coil connected to an engine rotating at 150 rpm. Some physical characteristics of the extruded PET fiber are summarized in **Table 1**.

2.2. Preparation of PLA/PET fiber composites

PET fibers were cut to the average length of 2-3mm, and then dried at 80°C for 24 hours. PLA pellets were also dried at 60°C for 24 h. PLA/PET fiber composites were prepared by adding 0.5, 1, 1.5, 2, 2.5 and 3 phr (parts per hundred parts) PET fibers to the PLA matrix by melt mixing at 180°C and 45 rpm for 15 minutes in a Brabender plasticorder®equipment (Duisburg, Germany).

2.3. Experimental techniques

2.3.1. Rheological and viscoelastic properties

The rheological behavior of PLA and PLA/PET fiber composites was studied by varying the mixing torque versus time during melt mixing in the internal mixer.

Neat PLA and PLA/PET fiber composites samples of dimensions 18 mm×10 mm×2mm were subjected to viscoelastic analysis in a DMA-Q800 equipment (TA Instruments, New Castle, DE, USA) in single cantilever geometry. Samples were heated from 40 to 120°C at a heating rate of 5°C/min. All experiments were carried out at a frequency of 1 Hz, an amplitude of 20 μm and a strain of 0.5%.

2.3.2. Structural analysis

2.3.2.1. Infrared spectroscopy

The chemical structures of the neat PLA, PET fiber and PLA/PET fiber composites were assessed by attenuated total reflectance-Fourier transform infra-red spectroscopy (ATR-FTIR) in a Tensor 27 spectrometer (Bruker Optik GmbH, Ettlinger, Germany) using a diamond prism. The angle of incidence of the IR beam was 45 degrees, and 60 scans were recorded and averaged at a resolution of 4 cm^{-1} in the wavenumber range 4000-400 cm^{-1}. Under these experimental conditions, a depth of the surface of about 10-15 μm was analyzed.

2.3.2.2. Contact angle measurements

The contact angles at 25 ºC were measured on the surfaces of the neat PLA and PLA/PET fiber composites in an ILMS goniometer (GBX Instruments, Bourg-de-Pèage, France) by using a polar (bi-distilled and deionized water) and a non-polar liquid (diiodomethane). A drop of water or diiodomethane was placed on the material surface and the contact angle was evaluated 5 minutes after drop deposition [37]. The contact angle values were calculated as the average of the values obtained with 3 drops placed in different location of the surface.

The surface energies (γ_S) of the neat PLA and PLA/PET fiber composites were determined from the water and diiodomethane contact angle values by using Owens-Wendt approach – equation (1):

$$\frac{(1+\cos\theta_i)\gamma_{li}}{\sqrt{\gamma_{li}^d}} = \sqrt{\gamma_s^P} + \sqrt{\frac{\gamma_{li}^P}{\gamma_{li}^d}}\sqrt{\gamma_s^d} \qquad \text{(Eq. 1)}$$

where γ_s^P and γ_s^d are, respectively, the polar and dispersive components of the surface energy, θ_i is the contact angle measured with each test liquid, and γ_{li}^P and γ_{li}^d are the polar and dispersive components of the surface tension of water and diiodomethane, respectively.

The work of adhesion was evaluated by using equation (2):

$$W_{adh} = 2(\gamma_s^d\gamma_L^d)^{\frac{1}{2}} + 2(\gamma_s^p\gamma_L^p)^{\frac{1}{2}} \qquad \text{(Eq. 2)}$$

2.3.3. Morphological analysis

2.3.3.1. X-ray diffraction (XRD)

The microstructures of the PLA, PET fiber and PLA/PET fiber composites were analyzed by wide X-ray diffraction in a Bruker D8-Advance diffractometer (Bruker, Ettlingen, Germany) equipped with a copper cathode and a nickel filter with Göbel mirror. The wavelength of Cu kα radiation (λ) - 0.1540598 nm – was used. XRD patterns were recorded from 0° to 60° in 0.05° steps acquired at a scan rate of 3°/min. The crystallites size (L) was calculated by using Scherrer's equation (equation (3)):

$$L = \frac{0.9\lambda}{\beta \cos\theta} \quad \text{(Eq. 3)}$$

where β and θ are, respectively, the bread at half-maximum intensity and the Bragg angle.

2.3.3.2. Scanning Electron Microscopy (SEM)

The morphology of the neat PLA and PLA/PET fiber composites was observed in a Hitachi S-3000N (Hitachi Ltd., Tokyo, Japan) scanning electron microscope, an electron beam energy of 15 kV was used. Izod impact fractured surfaces were analyzed by SEM which, for improving the contrast, were gold coated in a Balzers SCD 004 sputtering unit (Oerlikon Balzers, Liechtenstein). PET fiber morphology was analyzed in a Jeol NeoScope JMC-5000 scanning electron microscope (Jeol Ltd. Tokyo, Japan).

2.3.4. Thermal analysis

2.3.4.1. Differential scanning calorimetry (DSC)

DSC measurements were carried out in a Q100 DSC equipment (TA Instruments, New Castle, DE, USA), under nitrogen atmosphere (50 mL/min). 8-9 mg sample was placed in an aluminium pan and first heated from 0 to 200ºC, then cooled down to -80ºC at a cooling rate of 10ºC/min and finally it was re-heated from -80 to 250ºC. For both heating cycles, the rate was 10ºC/min. For PET fiber, the first heating run was carried out between 25 and 300ºC, then after cooling down to 25°C, a second heating cycle was performed to 300°C at 10ºC/min.

The glass transition temperature (T_g) and melting temperature (T_m) and enthalpy (ΔH_m) of the samples were assessed from the second DSC heating runs, whereas the crystallization temperature (T_c) and enthalpy (ΔH_c) were evaluated from the cooling runs. The degree of crystallinity (X_c) of the neat PLA and the composites was evaluated according to equation (4):

$$X_c = \frac{\Delta H}{\Delta H_m^0 \left(1 - \left(\frac{\omega t.\%_{\text{filler}}}{100}\right)\right)}.100 \quad \text{(Eq. 4)}$$

where ωt.% $_{filler}$ is the total weight fraction of the PET fibers into the composite, ΔH is either ΔH_c from the cooling curves or ΔH_m from the melting DSC curves. ΔH_m^0 is the melting enthalpy of the fully crystalline PLA (93 J/g) or PET (140 J/g) [38,39].

2.3.4.2. Thermal gravimetric analysis (TGA)

The thermal stability of PLA, PET fiber and PLA/PET fiber composites was evaluated in a TGA Q500 equipment (TA Instruments, New Castle, DE, USA) under nitrogen atmosphere (flow rate : 50 mL/min). 10-11 mg sample was placed in platinum crucible and then heated from 25 to 600°C at 10°C/min. The degradation parameters, including the temperatures at which starts (T_{d0}) and finishes (T_{fd}) the main decomposition, the temperature at maximum weight loss (T_{dmax}), the temperatures corresponding to the weight loss of 5% ($T_{5\%}$) and 50% ($T_{50\%}$), and the decomposition rate (V_d) were evaluated from the variations of the weight (TGA) and the derivative of the weight (DTGA) versus temperature.

2.4. Mechanical properties

Neat PLA and PLA/PET fiber composites unnotched specimens with dimensions of 63 mm×13 mm×2 mm were subjected to Izod impact test at room temperature in a Resil impact pendulum (Ceast, Italy). The apparatus consists of a heavy pendulum equipped with a hammer of 7.5 Kg inclined by a fingernail of 150° and a dial indicating the energy absorbed during the impact (A_n). Five samples were measured and averaged, the impact strength (a_n) was calculated according to equation (5):

$$a_n = \frac{A_n}{b.e} \qquad \text{(Eq. 5)}$$

where b and e are the width and the thickness of the test specimens, respectively.

3. Results and discussion

3.1. Rheological characterization of the PLA/PET fiber composites

The torque response of the neat PLA and PLA/PET fiber composites was recorded as a function of the mixing time (**Figure 1**). The torque of the neat PLA becomes stable at 5.4 N.m, and the addition of 1phr PET fiber induces a slight decrease of the torque value (4.6 N.m), this anticipates a good dispersion of the PET fibers into PLA matrix because the interactions between the PLA chains are attenuated, this is leading to lower melt viscosity value. However, the addition of 2 and 3 phr PET fiber increases the torque value to 5.7 and 6.6 N.m, respectively,

due to the creation of some rigid phases between the PLA matrix and the PET fibers leading to higher melt viscosity. The interactions between PLA and the PET fibers can be ascribed to the existence of hydroxyl and carboxyl groups in both polymers, which may create hydrogen bonds, this produces chains entanglement sites, which could oppose more resistance to the mixing process, and, consequently, more intensive shear forces are needed. Similar results have been reported earlier by Rahem et al. [12] in PLA/Luffa fiber composites compatibilized with anhydride maleic-grafted PLA, and they were ascribed to the affinity between PLA and Luffa fiber.

The viscoelastic behavior of the neat PLA and PLA/PET fiber composites was studied by DMTA. **Figures 2(a)** and **2(b)** show, respectively, the variations of the storage modulus (E´) and the damping factor (tan δ) versus temperature. At low temperature and below the glass transition region, the neat PLA is in the glassy state in which all chains are steady, and the storage modulus does not vary with the temperature (5156 MPa). At about 60°C, the glass transition of neat PLA starts and a decrease in the storage modulus is produced and it continues decreasing by increasing the temperature. When the T_g of PLA is attained, a maximum in tan δ at 86°C is produced (**Figure 2(b)**) and, after the glassy region, the chains mobility is favored, the polymer stiffness decreases and becomes more flexible. This leads to the decrease in the storage modulus until an almost constant value is obtained in the rubbery plateau region, then the melting is initiated.

When the PET fibers are added, the storage modulus of the neat PLA generally decreases, irrespective of the added amount; the composite with 2phr is an exception. The PLA/PET fiber composite containing 0.5 phr PET shows the lowest storage modulus and the glassy region is extended over large temperature range, an indication of the disruption of the interactions between the PLA chains. Furthermore, the decline of the storage modulus in the PLA/PET fiber composites containing 0.5 to 1.5 phr PET is due to matrix plasticization because the diluting effect induced by the PET fibers prevails over the PLA interactions, thus causing the matrix de-cohesion and a decrease in the stiffness. The addition of 2phr PET fiber causes an optimal dispersion in the PLA matrix due to more net interactions, which dominates over the fiber plasticizing effect. Consequently, a more net PET fiber/matrix interface is created, thus hindering the PLA chains mobility and causing an increase in the composite stiffness. Furthermore, the incorporation of higher PET fiber amounts (2.5 and 3phr) decreases more the storage modulus due to increased chains entanglements. Concomitantly, the fraction of free volume is enhanced and the extent of the interactions is drastically reduced because of the poor

wetting of the fibers by the matrix due to the higher fiber loading [36,40]. Beyond the glass transition region, the composite with 2phr PET fiber shows the highest storage modulus, this suggests that the stiffening caused by the interactions among the polymeric chains prevails over the diluting effect due to the addition of the fibers.

Additional valuable information on the changes in the viscoelastic properties of PLA induced by adding different amounts of PET fibers can be assessed from the examination of the tan δ value at the maximum of the peak (max tan δ) which temperature can be related to the T_g value. **Table 2** gathers the T_g and max tan δ values obtained from the damping factor vs temperature plots. The plot of tan δ of the neat PLA shows several structural relaxations at 50, 58, 70 and 86ºC (**Figure 2(b)** and **Table 2**) corresponding to different interactions between the PLA chains, the main one is located at 86ºC which can be associated to PLA glass transition temperature. The maxima tan δ in the composites vary between 0.04 and 0.19, and they increase with the temperature indicating higher dominance of the viscous component, the structural relaxation at 86ºC is an exception. The addition of 0.5 phr PET fiber decreases the tan δ and lower the tan δ value of the structural relaxation at 85ºC, thus pointing out to the intercalation of the PET fibers between the PLA chains. When 1 phr is added, one unique relaxation at 85 ºC with the highest tan δ value can be distinguished because of more net intercalation of the PET fibers between the PLA chains leading to the highest viscous component, i.e., the optimal balance between stiffness and toughness is obtained, this is related to its highest impact strength (see below). All PLA/PET composites containing 1phr or higher amounts PET fiber show one relaxation located at higher temperature than in PLA, this can be related to the improved matrix/fiber adhesion [21]. Thus, the composites with 1 and 2phr PET fiber present T_g values of 87-89°C due to more net interactions between the PLA and PET fiber chains and better interfacial adhesion. In PLA/2.5 phr PET fiber composite, the interactions between the polymeric chains could be efficiently developed (T_g value of 92°C), but the poor wetting of the PET fibers caused by their higher loading reduces the storage modulus. Finally, the addition of 3phr PET fiber decreases the T_g of the PLA phase due to a more important de-cohesion of the composite resulting from fibers agglomeration, the higher fraction of the free volume and the poor matrix/fiber adhesion, in agreement with the findings of Lopez-Manchado et al. [41] for polypropylene/PET fiber composites.

3.2. Impact strength and morphology of the PLA/PET fiber composites

The impact strength values of the neat PLA and PLA/PET fiber composites in **Figure 3** agree well with the DMA results. The impact strength of the composites increases when they contain

low PET fiber content, i.e. 0.5 and 1 phr, and decreases gradually by increasing the PET fiber amount. Indeed, the neat PLA exhibits an impact strength of 11.7 kJ/m², which increases to 13 kJ/m² by adding 0.5 and 1phr PET fiber, an increment by 11 %. Thereafter, the impact strength decreases to the lowest value of 8.7 kJ/m² in the composite with 3phr PET fibers. Therefore, for lower PET fibers loading, the fibers are well dispersed into the PLA matrix, this allows the creation of favorable interactions able to ensure an efficient stress transfer through the composite thanks to the interactions between the polymeric chains and their good interfacial adhesion. Besides, the PET fibers confer some toughness making the composites more resilient [36]. However, for higher PET fibers loading, the fibers aggregation due to fiber/fiber interactions is produced at the expense of the fiber/matrix interactions. Subsequently, the brittle fracture shown in the composites could be the result of multiple concomitant negative effects, such as the high proportion of voids and wetting imperfections resulting from the fibers pull-out.

Both PET fibers dispersion and interfacial adhesion were assessed from the SEM micrographs of the fractured surfaces of the composites (**Figure 4**). The PLA matrix (**Figure 4(a))** shows a relatively rough surface with short and irregular microcracks originated by imperfections and weak regions [42]. The PET fiber in **Figure 4(b)** exhibits a regular cylindrical shape with smooth surface and a diameter of 60-75 µm. The SEM micrograph of the PLA/1phr PET fiber composite (**Figure 4(c))** shows a good dispersion of the PET fibers which seem to be well trapped in the PLA matrix because of the interactions between the functional groups of both polymers and the absence of fibers agglomeration. Furthermore, the SEM micrograph shows the de-bonding of some fibers, and, even the clean aspect of the PET fibers surface, their extremities are stretched and flat, these evidences the role of the PET fibers in withstanding stresses solicitations and in dissipating energy during the composite rupture. This would not be observable if the fibers were not sufficiently anchored into the PLA matrix thanks to the interactions between the two polymers. The adequate PET fiber/matrix adhesion is also attested by the absence of notable gaps or voids at the interface, which would allow energy dissipation, as it has been noticed from the increased impact resistance of some composites containing PET fibers [43]. The increase in PET fiber loading generates entanglement sites, more noticeably for the composite with 3phr than with 2phr PET fiber (**Figure 4(d)-4(e))**, and because the poor wetting of the PET fibers by the matrix, several voids are evidenced in the SEM micrographs, those could be responsible for decreased resilience [36,44]. Hence, fiber de-bonding is

manifested in the PLA/3phr PET fiber composite because of the poor wetting and the parallel location of the fibers to the solicitation axis.

3.3. Structure of the PLA/PET fiber composites

To highlight the nature of the interactions between PLA and the PET fibers, the ATR-FTIR spectra of the neat PLA, PET fiber and PLA/PET fiber composites were obtained. **Figure 5** shows the ATR-IR spectrum of the neat PLA in which the C-H stretching at 2999-2923 cm^{-1} and the C=O stretching at 1748 cm^{-1} of the ester groups of PLA, can be noticed. The bands at 1455, 1348 and 1360 cm^{-1} correspond to the symmetric and asymmetric C-H bending in CH_3, the bands at 1181 and 1043 cm^{-1} are due to C-O and C-O-C stretching, and the bands at 957 and 872 cm^{-1} belong to O-H and C-O-C- groups, respectively [12]. On the other hand, the ATR-IR spectrum of the PET fiber shows the C-H stretching of the -CH_2 groups at 2962-2854 cm^{-1} and the C=O stretching band of the ester group appears at 1714 cm^{-1}. The bands at 1578, 1504 and 1456 cm^{-1} correspond to the C=C groups in the aromatic ring, and the in-plane bending of symmetric and asymmetric C-H groups appear at 1408 and 1338 cm^{-1}. Furthermore, -C-O-C- and -C-OH stretching at 1242 cm^{-1}, in-plane -CH bending of aromatic ring at 1095 cm^{-1}, -C-O stretching at 970 cm^{-1} and out- of-plane bending of C-H in aromatic ring and C-H deformation of bi-substituted aromatic ring at 873-723 cm^{-1} can also be distinguished [34].

The ATR-IR spectra of the PLA/PET fiber composites containing 1, 2 and 3 phr PET fibers are somewhat similar to the one of the neat PLA, this indicates the absence of chemical interactions between PLA and PET. However, the C-O band of the ester group at 1265 cm^{-1} and the one of the CH_3 groups at 1383 cm^{-1} are more intense indicating a structural change. The absence of chemical interactions in composites made with PET fibers has been evidenced elsewhere [34, 45, 46]. The polarities of the carboxyl and hydroxyl groups in both PLA and PET allow the occurrence of physical interactions, i.e., hydrogen bonding, which causes the PLA/PET miscibility [30-32, 34, 35]. Therefore, the adhesion in the interfacial region between the PET fibers and the PLA matrix can be ascribed to both hydrogen bonds and/or to electrostatic forces between the polar groups of both polymers [33, 34]. The hydrogen bonds between the hydroxyl groups of PLA and the carbonyl groups of the PET fibers, or between the oxygen of the -C=O group of PLA and the hydrogen of-CH_2 groups of the PET fiber are expected to be the main source of the physical interactions at the PLA/PET fiber interface (**Figure 6**).

Additionally, the contact angle values obtained by using polar and non-polar test liquids may provide additional insight into the surface changes induced by adding the PET fibers to PLA. The surface energies and their dispersive and polar components of PLA and the composites are

given in **Table 3**. PLA is a hydrophobic material with a weak polar character resulting from the low concentration of terminal polar groups, and, accordingly, PLA shows relatively high water and diiodomethane contact angle values (74 degrees and 53 degrees, respectively). Hence, PLA presents a low surface free energy (36 mJ/m²), which is mainly due to the dispersive component, in agreement with the literature [47-53]. The addition of the PET fibers decreases the hydrophobicity of PLA, the higher is the fiber content, the lower is the water contact angle value (θ_w decreases from 74 degrees on the neat PLA to 59 degrees on the composite with 3phr PET fibers). This suggests that, by increasing the PET fiber loading, the composites surface enriches in polar groups (-OH and -COOH) which enhances hydrophilicity [50], and, thus, the surface energies of the composites increase from 36 to 48 mJ/m². Likewise, the work of adhesion of the composites increases with the amount of PET fibers, thus corroborating their more hydrophilic surface [54-57]. These results support also the physical interactions involved at the interface between PLA and the PET fibers, as evidenced by ATR-IR spectroscopy, and in agreement with the literature [35].

3.4. Crystallinity of the PLA/PET fiber composites

The structure of the neat PLA, the PET fiber and the PLA/PET fiber composites were studied by DSC; the first heating, cooling and second heating DSC curves are displayed in **Figures 7(a), 7(b)** and**7(c)**, respectively and some of the thermal events are resumed in **Table 4**.

The second heating DSC curve of PLA shows the glass transition temperature at 61°C and two melting endotherms at 166 and 176 °C with melting enthalpy of about 62 J/g; the double melting peak of the neat PLA is common in polyesters and semi-crystalline polymers [58, 59] and is ascribed to the coexistence of two crystalline phases of α- orthorhombic and α'-pseudo-orthorombic structures presenting different thickness and degree of perfection [60, 61]. Also, the DSC cooling run of the neat PLA exhibits a cold crystallization exotherm at 112°C with an enthalpy of 59 J/g, which corresponds to a crystallinity degree of 67%. Furthermore, the second heating DSC curve of the PET fibers shows a T_g at 76 °C and a double melting peak at 244 and 251°C ascribed to two different crystalline phases, and a cold crystallization temperature at 207°C with an enthalpy of 55 J/g is noticed. The PET fibers have a crystallinity of 34%, which is lower than that of the PET fibers used by Franciszczak et al. [62].

A decrease of 4ºC in the T_g of the PLA phase is noticed for all composites, which corroborates the plasticizing effect evidenced by DMA and the impact resistance tests. The presence of the PET fibers causes some de-cohesion of the matrix, which attenuates the inter-chain interactions and increases the free volume between the PLA chains that facilitates their mobility. Similarly,

Rahem et al. [12] pointed out that the decrease in the T_g of the PLA could be ascribed to the decrease of the polymer cohesion and the increase of the free volume fraction caused by the addition of Luffa fibers. Also, the T_g values obtained from the DSC curves are different from those obtained by DMA (see above), the difference can be explained by the dissimilarity of the analyzing method and equipment [42, 63].

The cold crystallization temperatures of the PLA phase and the PLA/PET fiber composites do not significantly vary, contrary to the crystallinity degree, due to the perturbing effect that the fibers exert on the formation and growth of PLA crystals during the cooling cycle. Furthermore, the melting temperature and the crystallinity of the composites are unchanged after adding PET fibers, likely due to the fact that the physical interactions at the matrix/fiber interface are not prone to create a covering phase on the smooth fiber surface and allow transcrystallization to occur. This does not fit well with the role of nucleating agents of the natural fibers [12, 64]. Also, PLA presents a low crystallization rate and therefore, its crystallization process could be altered due to the significant delay in the chains motions during/after the establishment of interactions with the PET fibers. So, even though PLA crystallinity degree is not affected by the addition of the PET fibers, it seems that both crystals nucleation and growing are strongly altered, this leads to insufficient nucleation of the crystallites (i.e., small crystallites are formed).

To examine the composites crystalline microstructure, their X-ray diffractograms were obtained (**Figure 8**). The XRD pattern of the neat PLA displays a strong diffraction peak at $2\theta = 11.6°$ assigned to the (110) crystal lattice, this indicates the semi-crystalline structure of PLA, as confirmed by DSC [42]. Additional diffraction peaks at 2θ values of 14, 17.3, 20, 22.4, and 23.8 related to (103), (110/200), (203), (210), and (220) crystalline planes, respectively, are also observed in the XRD of the neat PLA, this is consistent with the presence of two crystalline structures, stereocomplex and homocrystallites of trigonal and pseudo-orthorhombic structures [65-67]. Furthermore, the XRD of the PET fibers displays atypical broad diffraction peak indicative of an almost amorphous nature, in agreement with the findings by Gorrasi et al. [68] and Sczymsczyk et al. [69].

The PLA composites with 1.5 and 2.5 phr PET fibers show a single intense and broad diffraction peak at $2\theta = 11.3\text{-}11.5°$. Therefore, the crystalline lattice of the PLA phase in the PLA/PET fiber composites is not affected by the addition of the PET fibers, but the crystallites size decreases markedly from 15 nm in the neat PLA to 0.29 nm in the composite with 0.5phr PET fibers, and to 0.55-0.60 nm for the other composites, PLA/2.5phr PET is an exception (1.22 nm) **(Table 5)**. As anticipated from the DSC results, the low density of the PET fibers allows the

introduction of a relatively high amount in the PLA matrix which perturbs strongly the proper growing of the nucleated crystals likely due to both the low crystallization rate of the matrix and the electrostatic interactions, which hinder severely the crystals growth.

3.5. Thermal stability of the PLA/PET fiber composites

PET is one of the polymers with higher thermal stability as compared to the most biopolymers, so its addition even in the form of fibers to other polymers is expected to enhance the thermal stability. The thermal stabilities of the PLA/PET fiber composites were assessed by thermal gravimetric analysis, the TGA and DTGA curves are shown in **Figures 9(a)** and **9(b)**, respectively. Some thermal degradation parameters (T_{d0}, T_{d5}, T_{d50}, T_{df}, T_{dmax} and T_{dmax}) obtained from the TGA curves are given in **Table 6**.

The degradation of PLA, the PET fiber and the PLA/PET fiber composites occurs in only one single step. For neat PLA, the decomposition starts at 280°C and finishes at 361°C with a mass loss rate of 2.3 %/min and a maximum temperature of decomposition of 351°C. On the other hand, the PET fibers still thermally stable until 347°C, a temperature at which PLA is totally decomposed. The decomposition of the PET fibers proceeds more steadily at 1.7%/min until around 500°C after having a 50% weight loss at 419°C. Accordingly, the thermal stability of the PLA/PET fibers composites rises uniformly with increasing the amount of the PET fibers, so, as compared to the neat PLA, T_{d0} goes from 280 to 282, 284 and 285°C for the composites with 1, 2 and 3phr PET fiber, respectively. T_{d5} also shifts to higher temperature values from 305°C for neat PLA to 311 and 316°C in the composites filled with 2 and 3phr PET fibers. Similarly, T_{df} increases gradually with the increase in the amount of PET fibers, from 361°C for neat PLA to 382, 400 and 430°C for the composites with 1, 2 and 3phrPET fiber, respectively. Also, the addition of the PET fiber accelerates moderately the weight loss of the composites, probably due to the reduction of the matrix cohesion, as already reported in section 3.2. All these results fit well with those reported previously for unsaturated polyester resin reinforced with recycled PET fibers [36].

In fact, the TGA curves confirm the potential of PET fibers in upgrading the thermal stability of PLA, even more effectively than other synthetic [22] or natural fibers [12] did. The improved thermal stability of the PLA/PET fiber composites is owed primarily to the higher inherent stability of the PET polymer, and the creation of matrix/fiber interfacial interactions. This later contributes in improving the matrix stability by inducing solely a marginal increase in the degradation rate from 2.3%/min for neat PLA to 2.6%/min for the composite with 3phr PET

fiber. In fact, Mofokeng et al. [40] reported that the interactions avoid interfacial impurities that may accelerate the decomposition process of the composites.

4. Conclusions

In this study, PET fibers have been manufactured by an extrusion/drawing process and their effectiveness in reinforcing a PLA matrix has been explored. The addition of the PET fibers into PLA offered advantageous compromises between stiffness and toughness in a different extent depending on the fibers loading.

The addition of 0.5-1.5 phr PET fibers increased the impact strength of PLA/PET fiber composites due to the electrostatic and/or hydrogen bond interactions between the hydroxyl and carboxylic functional groups in both polymer surfaces. When 2 phr PET fiber was added, the composite became stiffer with a resilience equivalent to that of the neat PLA matrix. Beyond this amount, the toughness and stiffness of the composites decreased because the formation of fibers agglomerates and the poor wettability by the matrix, these caused fibers de-bonding and gaps which deteriorated the composites properties. Apart from the predictable increased thermal stability, the PET fibers could also improve the PLA mechanical properties from a tough to a stiff material or vice-versa. For the applications in which a tough material is required, the composites with up to 1.5 phr PET fibers would be more suitable, but when a stiff material is needed, the composite with 2phrPET fiber could be more convenient. Finally, the addition of the PET fibers to the PLA matrix provided composites with upgraded thermal and mechanical properties thanks to the physical and electrostatic interactions involved at the interface between the two polymers without the need of adding compatibilizers or apply treatments to the fibers.

References

[1] Assarar M, Scida D, El Mahi A, et al. Influence of water ageing on mechanical properties and damage events of two reinforced composite materials: flax–fibres and glass–fibres. Mater Des. 2011;32:788-795.

[2] Avérous L, Pollet E. Macro-, Micro-, and nanocomposites based on biodegradable polymers. In: Thomas S, Durand D, Chassenieux Ch, Jyotishkumar P, editors. Handbook of biopolymer-based materials. Weinheim (DE): Wiley; 2013. p. 173-210.

[3] Thori P, Sharma P, Bhargava M. An approach of composite materials in industrial machinery: advantages, disadvantages and applications. Int J Res Eng Technol. 2013;2:350-355.

[4] Siakeng R, Saba N, Jawaid M, et al. Natural fiber reinforced polylactic acid composites: a review. Polym Compos. 2018;40:446-463.

[5] Murawski A, Diaz R, Inglesby S, et al. Synthesis of bio-based polymer composites: fabrication, filler, properties, and challenges. In: Sadasivuni KK, Ponnamma D, Rajan M, Ahmed B, Al-Maadeed MASA, editors. Polymer nanocomposites in biomedical engineering. Switzerland (CH): Springer; 2019.p. 29-55.

[6] European Parliament and Council Directive. Requirements for packaging recoverable through composting and biodegradation – Test scheme and evaluation criteria for the final acceptance of packaging, EN 13432: 2000.

[7] Orue A, Jauregi A, Peña-Rodriguez C. et al. The effect of surface modifications on sisal fiber properties and sisal/poly (lactic acid) interface adhesion. Compos Part B Eng. 2015;73:132-138.

[8] Yu T, Hu Ch, Chen X. et al. Effect of diisocyanates as compatibilizer on the properties of ramie/poly(lactic acid) (PLA) composites. Compos Part A Appl Sci Manuf. 2015;76:20-27.

[9] Auras R, Lim LT, Selke SEM, et al. Poly (lactic acid) synthesis, structures, properties, processing, and applications. New Jersey (NJ): Wiley;2010.

[10] Bohlmann GM, General characteristics, processability, industrial applications and market evolution of biodegradable polymer. In: Bastioli C. editor. Handbook of biodegradable polymers. United Kingdom (UK): Rapra Technology; 2005. p183-217.

[11] Rasal RM, Janorkar AV, Hirt DE. Poly (lactic acid) modifications. Prog Polym Sci. 2010;35:338-356.

[12] Rahem Z, Mayouf I, Guessoum M, et al. Compatibilization of biocomposites based on sponge-gourd natural fiber reinforced poly(lactic acid). Polym Compos. 2019;40:4489-4499.

[13] Yang Y, Zhang L, Xiong Z, et al. Research progress in the heat resistance, toughening and filling modification of PLA. Sci China Chem.2016;59:1355-1368.

[14] Wan YZ, Wang YL, Li QY et al. Influence of surface treatment of carbon fibers on interfacial adhesion strength and mechanical properties of PLA-based composites. J Appl Polym Sci. 2001; 80:367-376.

[15] Bedreddine M, Nekkaa S, Guessoum M. Poly (lactic acid)/*Spartiumjunceum* fibers biocomposites: effects of the fibers content and surface treatments on the

microstructure and thermo-mechanical properties. Compos Interfaces. 2019;26:1101-1121.

[16] Wang G, Zhang D, Li B, et al. Strong and thermal-resistance glass fiber-reinforced polylactic acid (PLA) composites enabled by heat treatment. Int J Biol Macromol. 2019;129:448-459.

[17] Kim HS, Park BH, Choi JH, et al. Mechanical properties and thermal stability of poly(l-lactide)/calcium carbonate composites. J Appl Polym Sci. 2008;109:3087-3092.

[18] Murariu M, Dubois Ph. PLA composites: from production to properties. Adv Drug Deliv Rev. 2016;107:17-46.

[19] Kim JK, Mai YW. Engineered interfaces in fiber reinforced composites. Oxford (UK): Elsevier; 1998.

[20] Samouh Z, Molnar K, Boussu F, et al. Mechanical and thermal characterization of sisal fiber reinforced polylactic acid composites. Polym Adv Technol. 2019;30:529-537.

[21] Nanthananon Ph, Seadan M, Pivsa-Art S, et al. Reactive compatibilization of short-fiber reinforced poly(lactic acid) biocomposites. J Renew Mater. 2018;6:573-583.

[22] Wang G, Zhang D, Wan G, et al. Glass fiber reinforced PLA composite with enhanced mechanical properties, thermal behavior, and foaming ability. Polymer. 2019;181: 121803.

[23] Xiu H, Qi X, Liu Z, et al. Simultaneously reinforcing and toughening of polylactide/ carbon fiber composites via adding small amount of soft poly(ether)urethane. Compos Sci Technol. 2016;127:54-61.

[24] Lin JH, Huang CL, Chen ChK, et al. Manufacturing and mechanical property evaluations of PLA/carbon fiber/glass fiber composites. Appl Mech Mater. 2015;749: 261-264.

[25] Hsieh ChT, Pan YJ, Lou ChW, et al. Poly (lactic acid)/carbon fiber composites: effects of functionalized elastomers on mechanical properties, thermal behavior, surface compatibility, and electrical characteristics. Fibers Polym. 2016;17:615-623.

[26] Reese G. Polyester fibers: fiber formation and end-use applications. In: Scheirs J, Long TE, editors. Modern polyesters: chemistry and technology of polyesters and copolyesters. Chichester (UK): Wiley; 2003. p. 408-409.

[27] Saujanya C, Radhakrishnan S. Structure development and properties of PET fibre filled PP composites. Polymer. 2001;42:4537-4548.

[28] Irwan JM, Asyraf RM, Othman N, et al. The mechanical properties of PET fiber reinforced concrete from recycled bottle wastes. Adv Mater Res. 2013;795:347-351.

[29] Kim SB, Yi NH, Kim HY, et al. Material and structural performance evaluation of recycled PET fiber reinforced concrete. Cem Concr Compos. 2010;32:232-240.

[30] Chen H, Pyda M, Cebe P. Non-isothermal crystallization of PET/PLA blends. Thermochim Acta. 2009;492:61-66.

[31] Acar I, Pozan GS, ÖzgümüşS. Thermal oxidative degradation kinetics and thermal properties of poly(ethylene terephthalate) modified with poly(lactic acid). J Appl Polym Sci. 2008;109:2747-2755.

[32] You X, Snowdon MR, Misra M, et al. Biobased poly(ethylene terephthalate)/poly(lactic acid) blends tailored with epoxide compatibilizers. J Am Chem Soc. 2018;3:11759-11769.

[33] Torres-Huerta AM, Palma-Ramírez D, Domínguez-Crespo MA, et al. Comparative assessment of miscibility and degradability on PET/PLA and PET/chitosan blends. Eur Polym J. 2014;61:285-299.

[34] Torres-Huerta AM, Del Angel-López D, Domínguez-Crespo MA, et al. Morphological and mechanical properties dependence of PLA amount in PET matrix processed by single-screw extrusion. Polym Plast Technol Eng. 2016;55:672-683.

[35] McLauchlin AR, Ghita OR. Studies on the thermal and mechanical behavior of PLA-PET blends. J Appl Polym Sci. 2016;133:1-11.

[36] Dehas W, Guessoum M, Douibi A, et al. Thermal, mechanical, and viscoelastic properties of recycled poly(ethylene terephthalate) fiber reinforced unsaturated polyester composites. Polym Compos. 2016;39:1682-1693.

[37] Fuensanta M, Martín-Martínez JM. Thermoplastic polyurethane pressure sensitive adhesives made with mixtures of polypropylene glycols of different molecular weights. Int J Adhes Adhes. 2019; 88: 81-90.

[38] Garlotta D. A literature review of poly(lactic acid). J Polym Environ. 2001;9:63-84.

[39] Rahem Z, Douibi A, Lallam A, et al. Synergistic combination of crystallization and addition of a toughening agent to promote recycled poly(ethylene terephthalate) performances. Polym Sci Ser A Polym Chem. 2019;61:635-649.

[40] Mofokeng JP, Luyt AS, Tàbi T, et al. Comparison of injection moulded, natural fibre-reinforced composites with PP and PLA as matrices. J Thermoplast Compos Mater. 2012;25:927-948.

[41] López-Manchado MA, Arroyo M. Thermal and dynamic mechanical properties of polypropylene and short organic fiber composites. Polymer. 2000;41:7761-7767.

[42] Mayouf I, Guessoum M, Fuensanta M, et al. Appraisal of ε-caprolactam and trimellitic anhydride potential as novel chain extenders for poly(lactic acid). PolymEngSci2020;60:944-955.

[43] Huda MS, Drzal LT, Mohanty AK, et al. Chopped glass and recycled newspaper as reinforcement fibers in injection molded poly(lactic acid) (PLA) composites: a comparative study. Compos Sci Technol. 2006;66:1813-1824.

[44] Asaithambi B, Ganesan G, Ananda Kumar S. Bio-composites: development and mechanical characterization of banana/sisal fibre reinforced poly lactic acid (PLA) hybrid composites. Fibers Polym. 2014;15:847-854.

[45] Paszkiewicz S, Szymczyk A, Pawlikowska D, et al. Synthesis and characterization of poly(ethylene terephthalate-co-1,4 cyclohexane dimethyleneterephtlatate)-block- poly (tetramethylene oxide) copolymers. RSC Adv. 2017;7:41745-41754.

[46] Chieng BW, Ibrahim NA, YunusWM, et al. Poly(lactic acid)/poly(ethylene glycol) polymer nanocomposites: effects of graphene nanoplatelets. Polymers. 2014;6:93-104.

[47] Li D, Jiang Y, Lv Sh, et al. Preparation of plasticized poly (lactic acid) and its influence on the properties of composite materials. PLoS ONE, 2018;13:1-15.

[48] Magiera A, Markowski J, Menaszek E, et al. PLA-based hybrid and composite electrospun fibrous scaffolds as potential materials for tissue engineering. J Nanomater. 2017; ID 9246802:1-11.

[49] Sousa S, Costa A, Silva A, et al. Poly(lactic acid)/cellulose films produced from composite spheres prepared by emulsion-solvent evaporation method. Polymers, 2019;11:1-19.

[50] Gutierrez-Villarreal MH, Rodríguez-Gonzalez FJ, Perera-Mercado Y, Estimation of surface free energy of poly (lactic acid) during UV-grafting with N-vinylpyrrolidone. Macromol Symp. 2017;374:1-3.

[51] JiaSh, Yu D, Zhu Y, et al. Morphology, crystallization and thermal behaviors of PLA-based composites: wonderful effects of hybrid GO/PEG via dynamic impregnating. Polymers. 2017;9:1-18.

[52] Navarro M, Engel E, Planell JA, et al. Surface characterization and cell response of a PLA/CaP glass biodegradable composite material. J Biomed Mater Res. 2007;85A:477-486.

[53] Chitrattha S, Phaechamud Th. Film properties of poly (lactic acid) comprising n-methyl-2-pyrrolidone. Adv Mater Res. 2012;528:140-143.

[54] Mallikarjunachari G, Ghosh P. Analysis of strength and response of polymer nano thin film interfaces applying nanoindentation and nanoscratch techniques. Polymer. 2016;90:53-66.

[55] Biresaw G, Carriere CJ. Correlation between mechanical adhesion and interfacial properties of starch/biodegradable polyester blends. J Polym Sci B Polym Phys. 2001; 39: 920-930.

[56] Anastasiadis SH, Hatzikiriakos SG. The work of adhesion of polymer/wall interfaces and its association with the onset of wall slip. J Rheol. 1998; 42:795-812.

[57] Chin P, McCullough RL, Wu WL. An improved procedure for determining the work of adhesion for polymer-solid contact. J Adhes. 1997;64:145-160.

[58] Arruda LC, Magaton M, Bretas RES, et al. Influence of chain extender on mechanical, thermal and morphological properties of blown films of PLA/PBAT blends. Polym Test. 2015;43:27-37.

[59] Najafi N, Heuzey MC, Carreau PJ. Crystallization behavior and morphology of polylactide and PLA/clay nanocomposites in the presence of chain extenders. Polym Eng Sci. 2013;53:1053-1064.

[60] Medjdoub N, Guessoum M, Fois M. Viscoelastic, thermal and environmental characteristics of poly(lactic acid), linear low density polyethylene and low-density polyethylene ternary blends and composites. J Adhes Sci Technol. 2017;31:787-805.

[61] Chelghoum N, Guessoum M, Fois M, et al. Contribution of catalytic transesterification reactions to the compatibilization of poly(lactic acid)/ polycarbonate blends: thermal, morphological and viscoelastic characterization. J Polym Environ. 2018 ;26 :342-354.

[62] Francszczak P, Merijs-Meri R, Kalniņš K, et al. Short-fibre hybrid polypropylene composites reinforced with PET and Rayon fibres-Effects of SSP and interphase tailoring. Compos Struct. 2017;181:121-137.

[63] Giita Silverajah VS, Ibrahim NA, Zainuddin N, et al. Mechanical, thermal and morphological properties of poly(lactic acid)/epoxidized palm olein blend. Molecules. 2012;17:11729-11747.

[64] Bouzidi F, Guessoum M, Fois M, et al. Viscoelastic, thermo-mechanical and environmental properties of composites based on polypropylene/poly(lactic acid) blend and copper modified nanoclay. J Adhes Sci Technol. 2018;32:496-515.

[65] Xu JZ, Li Y, Li YK, et al. Shear-induced stereocomplex cylindrites in polylactic acid racemic blends: Morphology control and interfacial performance. Polymer. 2018;140:179-187.

[66] Baimark Y, Kittipoom S. Influence of chain-extension reaction on stereo-complexation, mechanical properties and heat resistance of compressed stereocomplex-polylactide bioplastic films. Polymers. 2018;10:1-10.

[67] Cui L, Wang Y, Guo Y, et al. Effects of temperature and external force on the stereocomplex crystallization in poly(lactic acid) blends. Adv Polym Technol. 2016;37:962-967.

[68] Gorrasi G, Milone C, Piperopoulos E, et al. Preparation, processing and analysis of physical properties of calcium ferrite-CNTs/PET nano-composite. Compos B Eng 2015;81:44-52.

[69] Szymczyk A, Paszkiewicz S, Pawelec I, et al. Oxygen barrier properties and melt crystallization behavior of poly(ethylene terephthalate)/graphene oxide nanocomposites. J Nanomater. 2015; ID 382610:1-11.

491

492

Table 1. Some physical properties of the PET fibers

Property	Value
Apparent density at 20°C (g/cm^3)	0.65
Number Metric (Nm)	200
Linear density (Dtex)	50
Fineness (Denier)	45
Diameter (µm)	60-75

Table 2. Values of temperature and maximum tan δ, and storage modulus (at 40°C) of the neat PLA and the PLA/PET fiber composites. DMA experiments.

Composite	T (°C)	Max tan δ	E´ at 40 ºC (MPa)
PLA	86	0.19	5156
PLA/0.5phr PET fiber	85	0.16	2547
PLA/1phr PET fiber	85	0.22	4419
PLA/1.5phr PET fiber	89	0.14	3244
PLA/2phr PET fiber	87	0.19	5333
PLA/2.5phr PET fiber	92	0.15	2759
PLA/3phr PET fiber	85	0.20	3844

Table 3. Water and diiodomethane contact angle at 25ºC, surface energy and work of adhesion values for neat PLA and PLA/PET fiber composites.

Composite	Contact angle (degrees)		Surface energy (mJ/m^2)			Work of adhesion (mJ/m^2)
	θ_w	θ_i	γ_s^p	γ_s^d	γ_s	W_{adh}
PLA	74 ±1	53 ±1	10	26	36	92
PLA/0.5phr PET fiber	69 ±1	46 ±1	11	29	40	97
PLA/1phr PET fiber	69 ±1	48±1	12	28	40	98
PLA/1.5phr PET fiber	70 ±1	46±1	11	29	40	97
PLA/2phr PET fiber	65 ±1	41 ±1	13	31	44	103
PLA/2.5phr PET fiber	62 ±1	39 ±1	14	31	46	105
PLA/3phr PET fiber	59 ±1	37 ±1	16	32	48	109

548

549

550

551

552

553

554 **Table 4.** Thermal events of neat PLA, PET fiber, and PLA/PET fiber composites. DSC

555 experiments.

Composite	Cooling run			2nd heating run				
	T_c (°C)	ΔH_c (J/g)	χ_c (%)	T_g (°C)	T_{m1} (°C)	T_{m2} (°C)	ΔH_m (J/g)	χ_c (%)
PLA	112	59	63	61	166	176	62	67
PET fiber	207	55	39	76	244	251	48	34
PLA/0.5phr PET fiber	111	54	58	59	169	175	62	67
PLA/1phr PET fiber	111	53	58	58	169	176	62	67
PLA/1.5phr PET fiber	111	52	57	57	168	175	61	67
PLA/2phr PET fiber	111	52	57	58	169	176	59	65
PLA/2.5phr PET fiber	111	51	56	56	167	174	60	66
PLA/3phr PET fiber	111	51	56	57	169	176	60	66

556

557

558

559

560

561

562

563

564

565

Table 5. Main X-ray diffraction peak and PLA phase crystallites size in the neat PLA and the PLA/PET fiber composites.

Composite	2θ (°)	L (nm)
Neat PLA	11.6	15.00
PET fiber	19.2	0.13
PLA/0.5phr PET fiber	11.7	0.29
PLA/1phr PET fiber	11.3	0.56
PLA/1.5phr PET fiber	11.5	0.60
PLA/2phr PET fiber	11.5	0.59
PLA/2.5phr PET fiber	11.5	1.22
PLA/3phr PET fiber	11.5	0.55

Table 6. TGA results for neat PLA, PET fiber and PLA/PET fiber composites.

Composite	T_{d0} (°C)	$T_{5\%}$ (°C)	$T_{50\%}$ (°C)	T_{dmax} (°C)	T_{df} (°C)	m_{loss} at T_{max} (%)	V_d (%/min)
PLA	280	305	344	351	361	31	2.3
PET fiber	347	381	419	419	500	50	1.7
PLA/1phr PET fiber	282	310	345	350	382	36	2.3
PLA/2phr PET fiber	284	311	345	350	400	35	2.5
PLA/3phr PET fiber	285	316	346	350	430	38	2.6

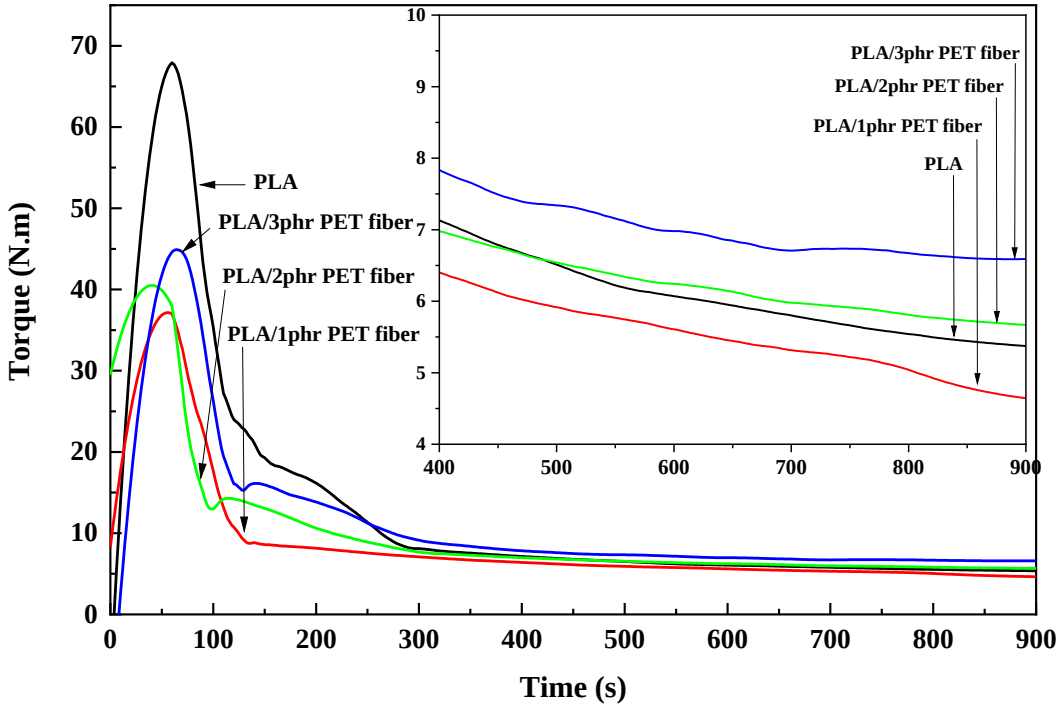
Torque (N.m)
Time (s)
PLA
PLA/3phr PET fiber
PLA/2phr PET fiber
PLA/1phr PET fiber
PLA/3phr PET fiber
PLA/2phr PET fiber
PLA/1phr PET fiber
PLA

Figure 1.

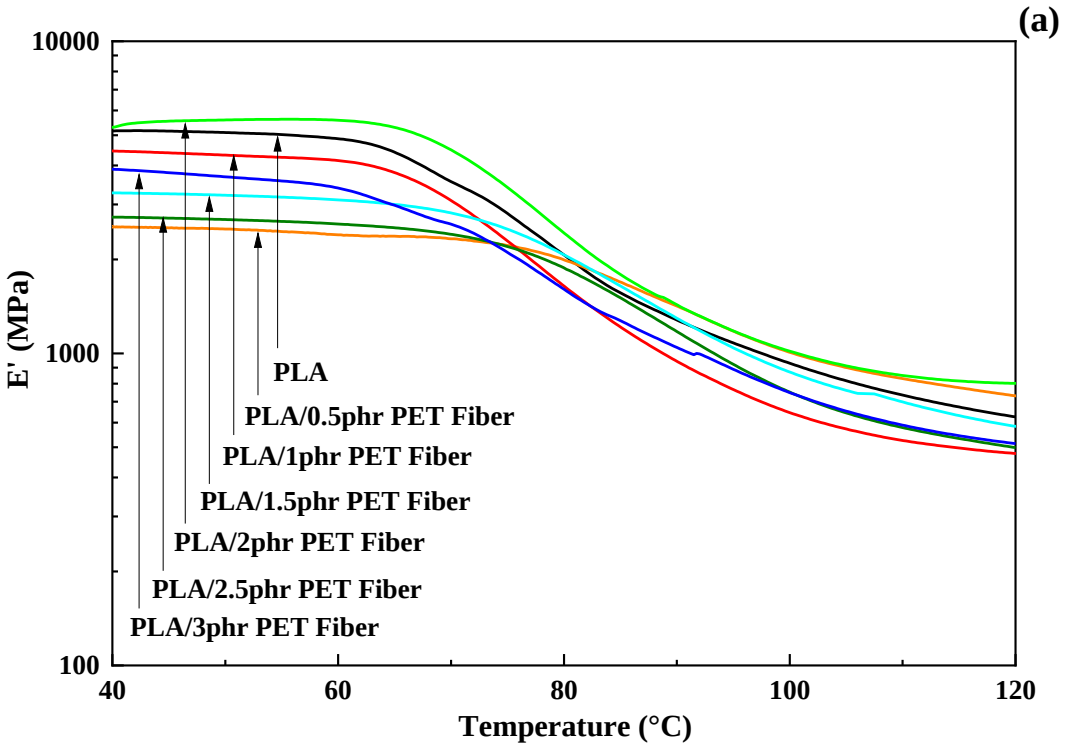

629 **Figure 2(a).**

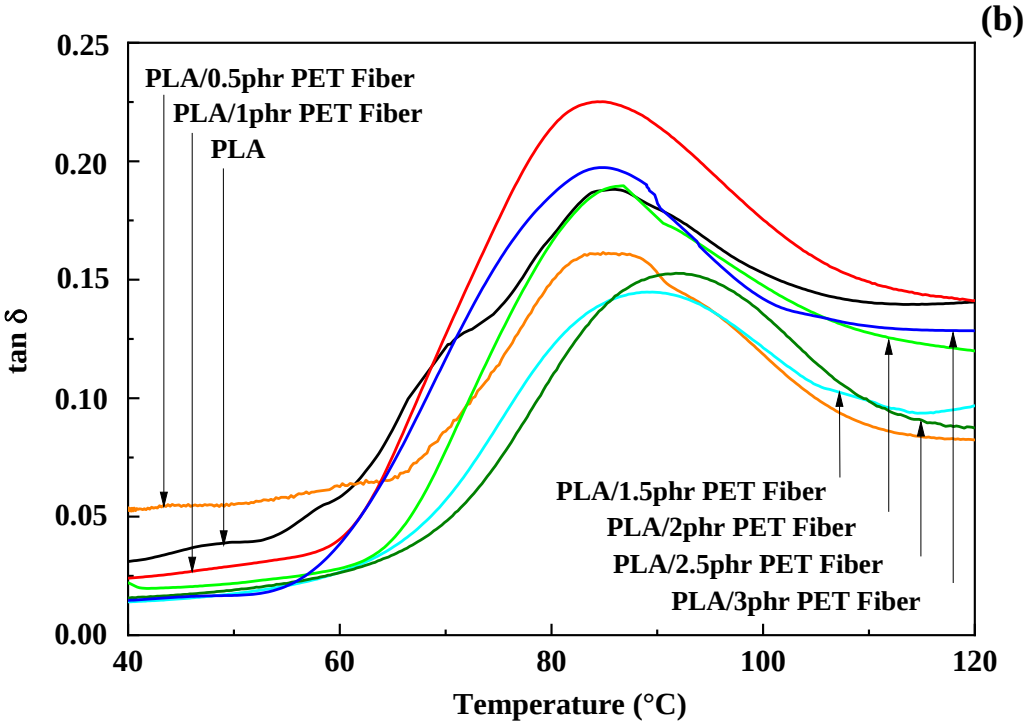

630 **Figure 2 (b).**

631

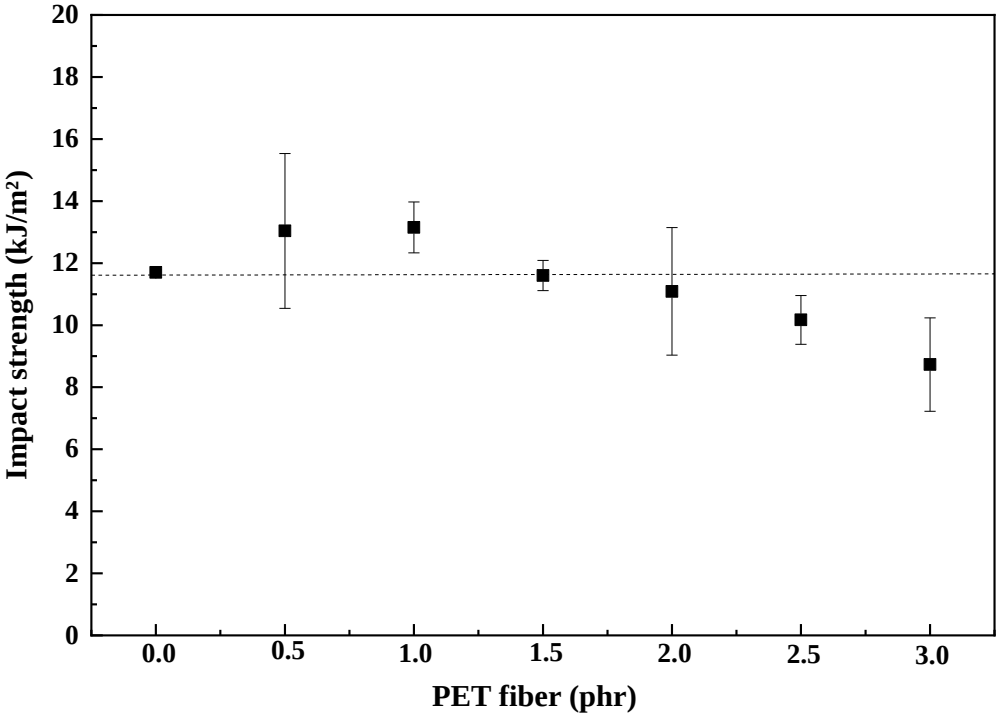
Impact strength (kJ/m²)
20
18
16
14
12
10
8
6
4
2
0
0.0
0.5
1.0
1.5
2.0
2.5
3.0
PET fiber (phr)

Figure 3.

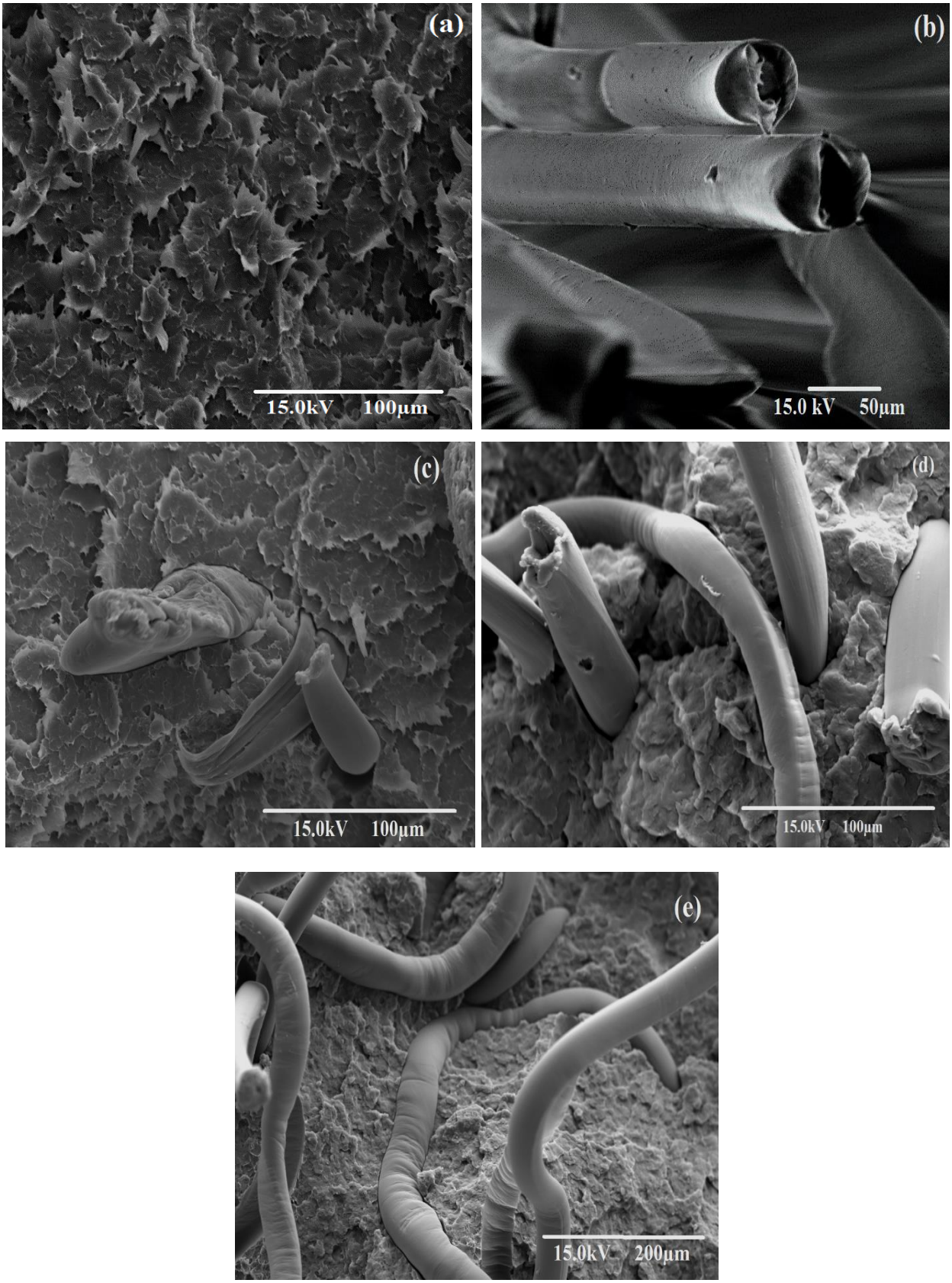

647 **Figure 4.**

648

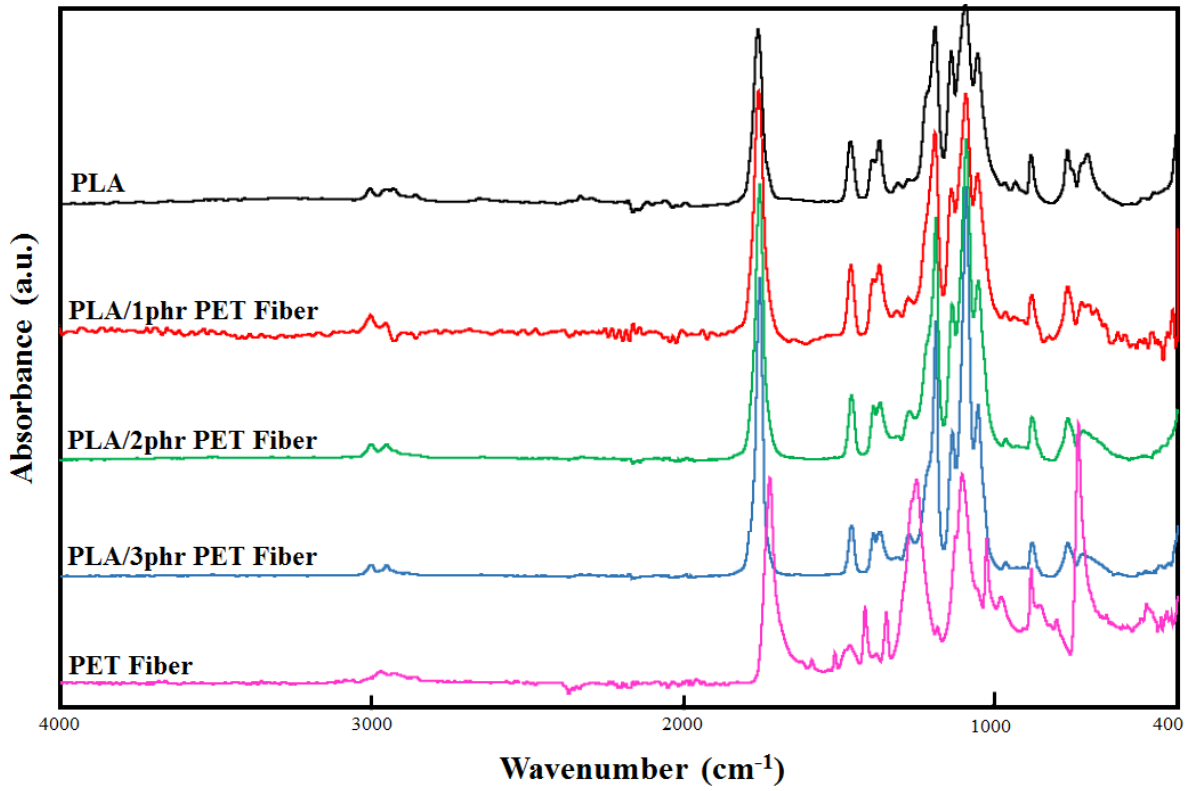

649 **Figure 5.**

650

651

652

653

654

655

656

657

658

659

660

661

662

663

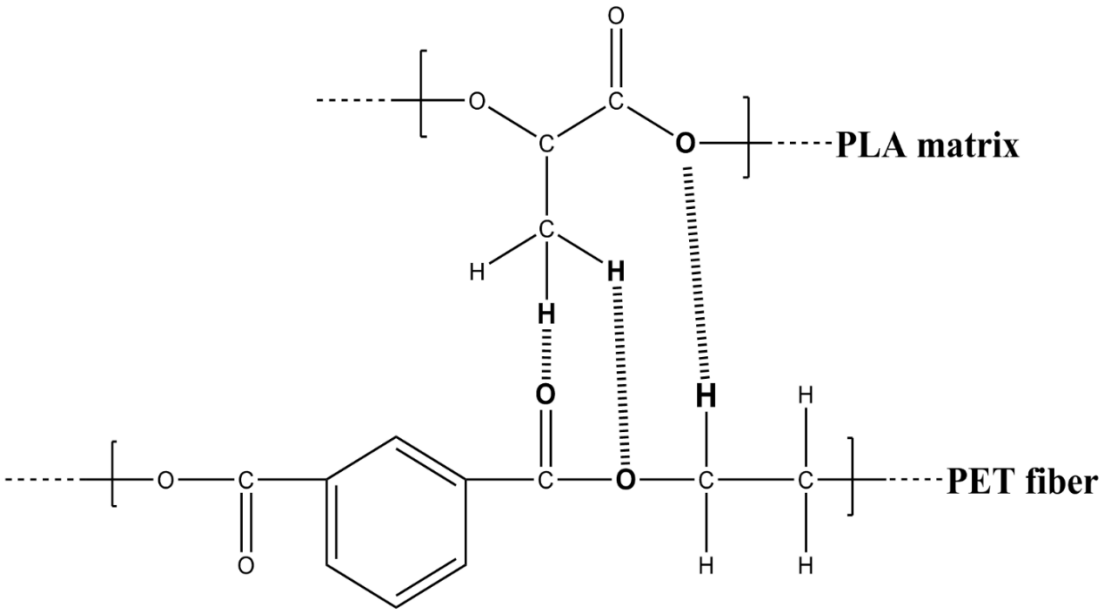

Figure 6.

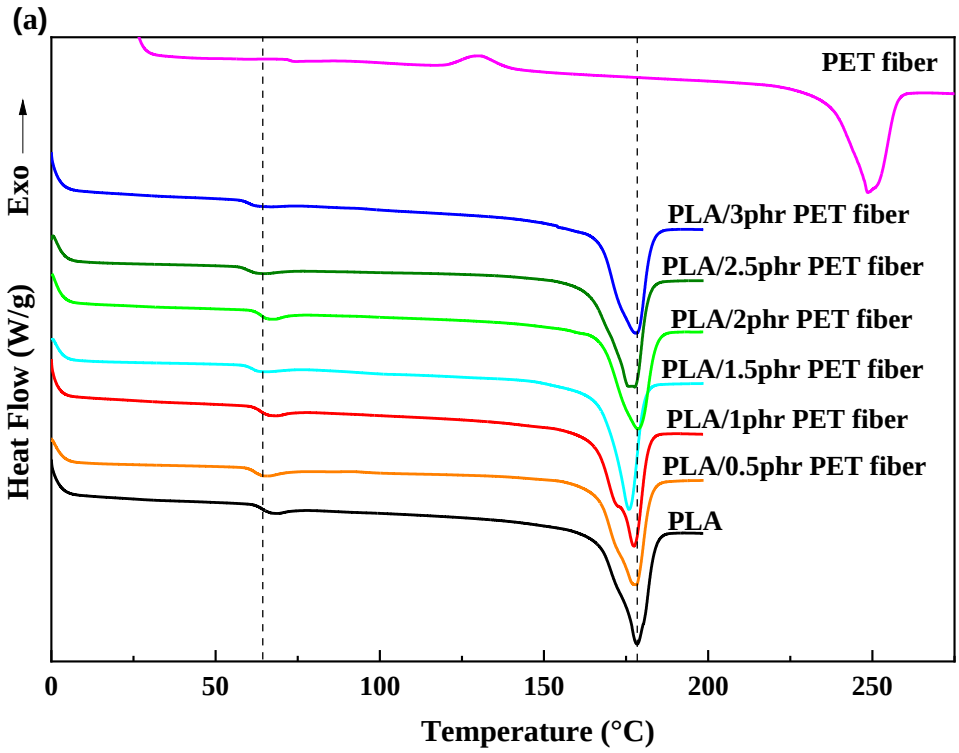
(a)
PET fiber
Exo
Heat Flow (W/g)
PLA/3phr PET fiber
PLA/2.5phr PET fiber
PLA/2phr PET fiber
PLA/1.5phr PET fiber
PLA/1phr PET fiber
PLA/0.5phr PET fiber
PLA
0
50
100
150
200
250
Temperature (°C)

Figure 7(a).

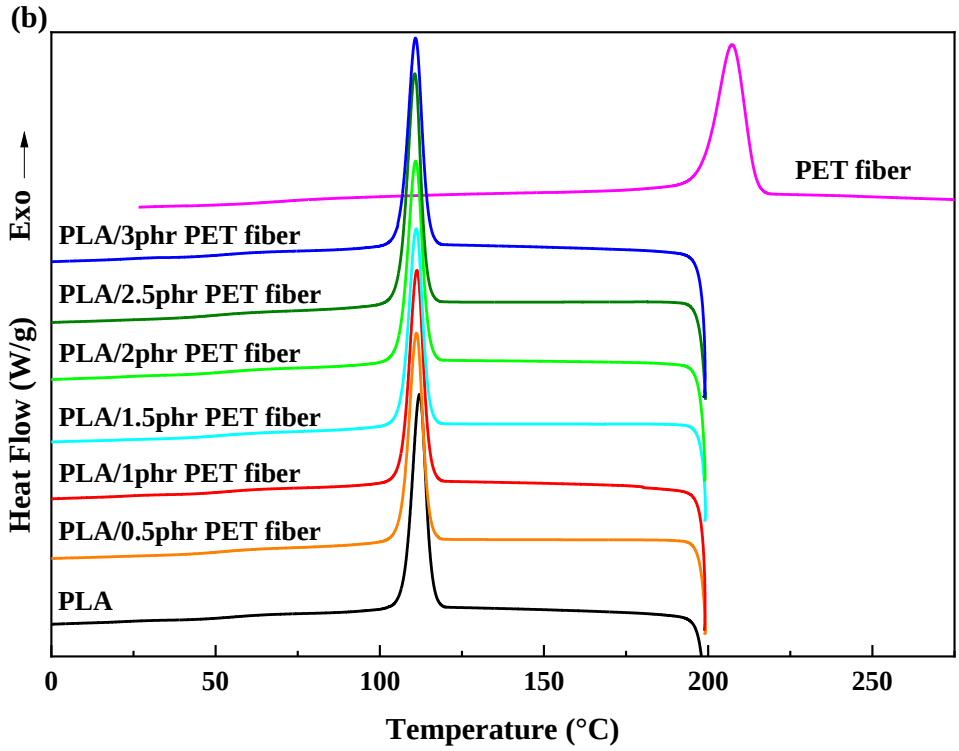
(b)
Exo
Heat Flow (W/g)
PET fiber
PLA/3phr PET fiber
PLA/2.5phr PET fiber
PLA/2phr PET fiber
PLA/1.5phr PET fiber
PLA/1phr PET fiber
PLA/0.5phr PET fiber
PLA
0
50
100
150
200
250
Temperature (°C)

Figure 7(b).

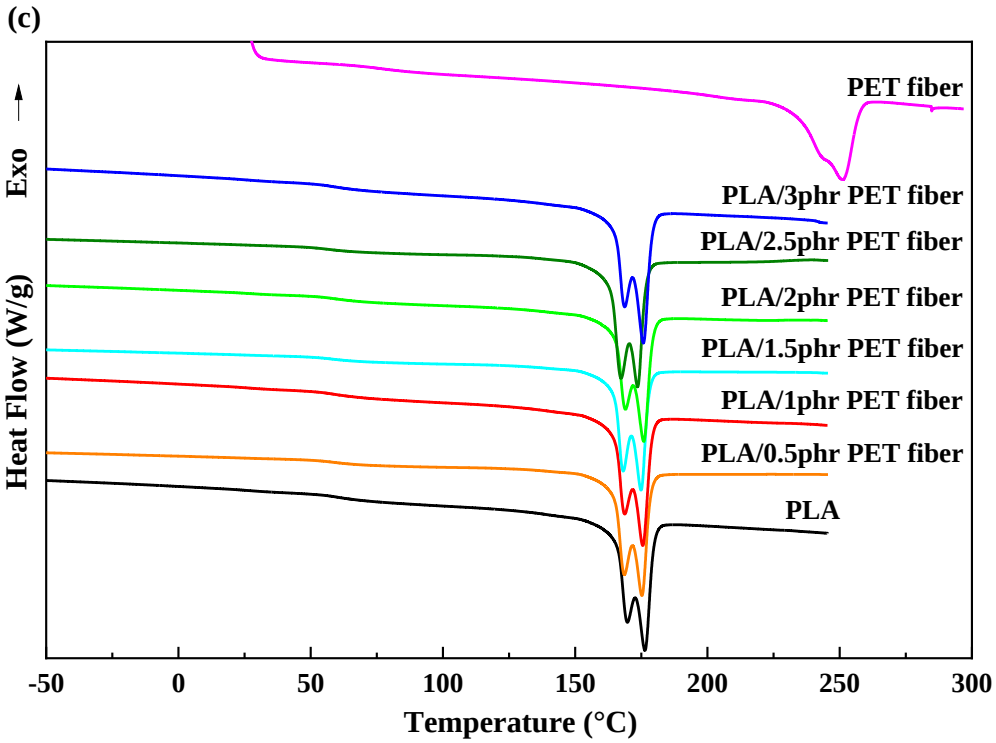
(c)
Exo
Heat Flow (W/g)
PET fiber
PLA/3phr PET fiber
PLA/2.5phr PET fiber
PLA/2phr PET fiber
PLA/1.5phr PET fiber
PLA/1phr PET fiber
PLA/0.5phr PET fiber
PLA
-50
0
50
100
150
200
250
300
Temperature (°C)

Figure 7(c).

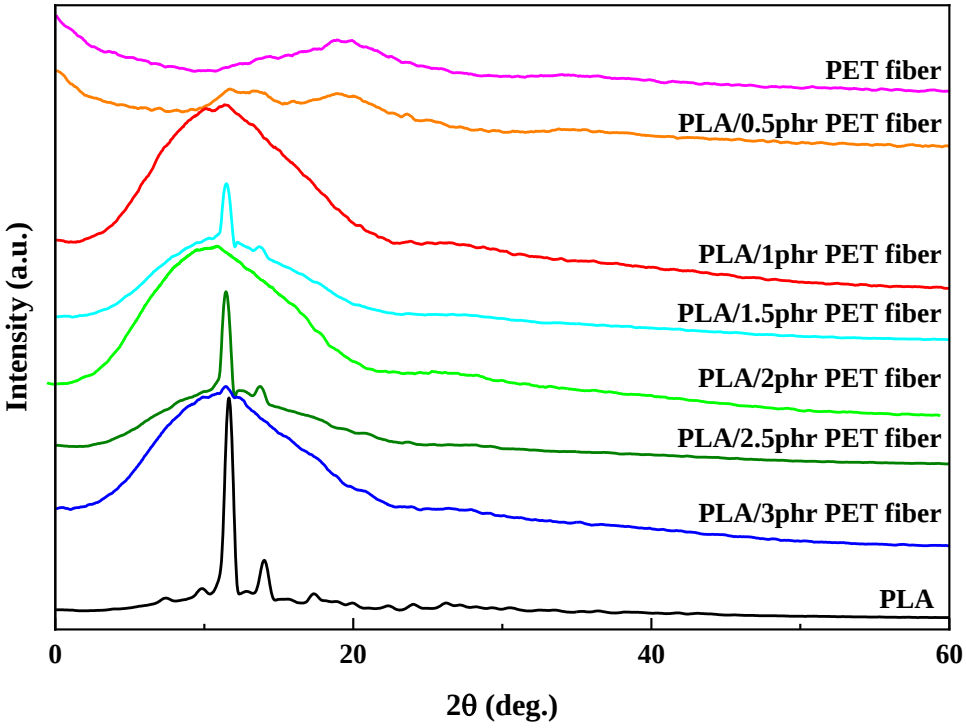
PET fiber
PLA/0.5phr PET fiber
PLA/1phr PET fiber
PLA/1.5phr PET fiber
PLA/2phr PET fiber
PLA/2.5phr PET fiber
PLA/3phr PET fiber
PLA
Intensity (a.u.)
0
20
40
60
2θ (deg.)

Figure 8.

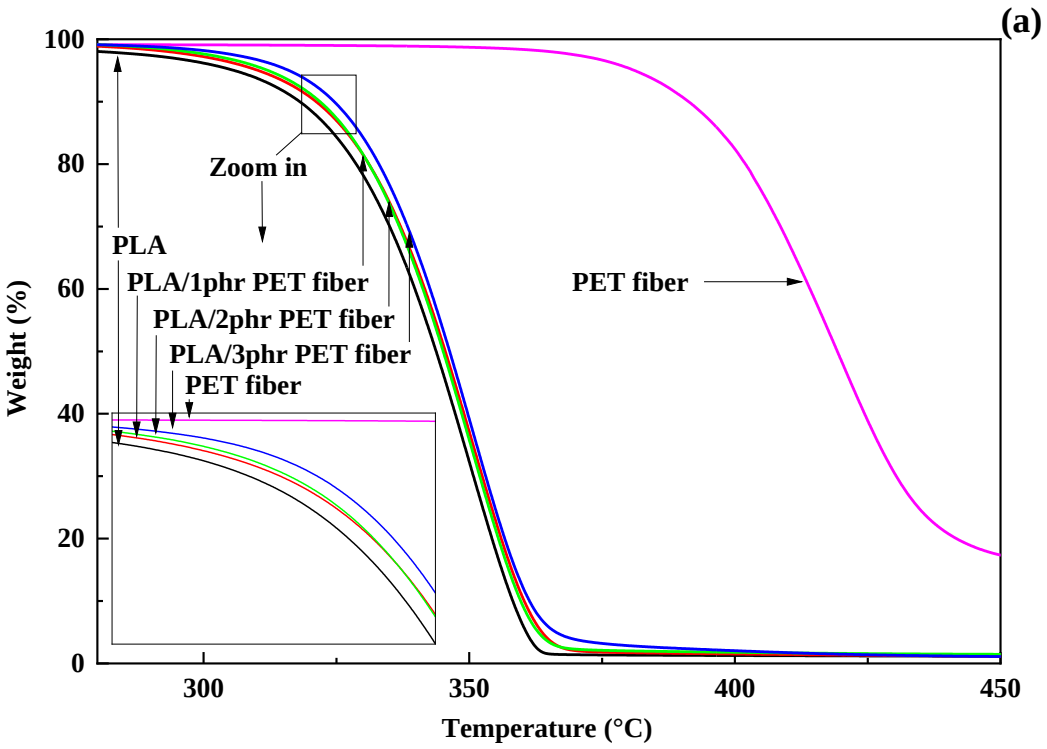
(a)
100
80
60
40
20
0
Weight (%)
300
350
400
450
Temperature (°C)
Zoom in
PLA
PLA/1phr PET fiber
PLA/2phr PET fiber
PLA/3phr PET fiber
PET fiber
PET fiber

Figure 9(a).

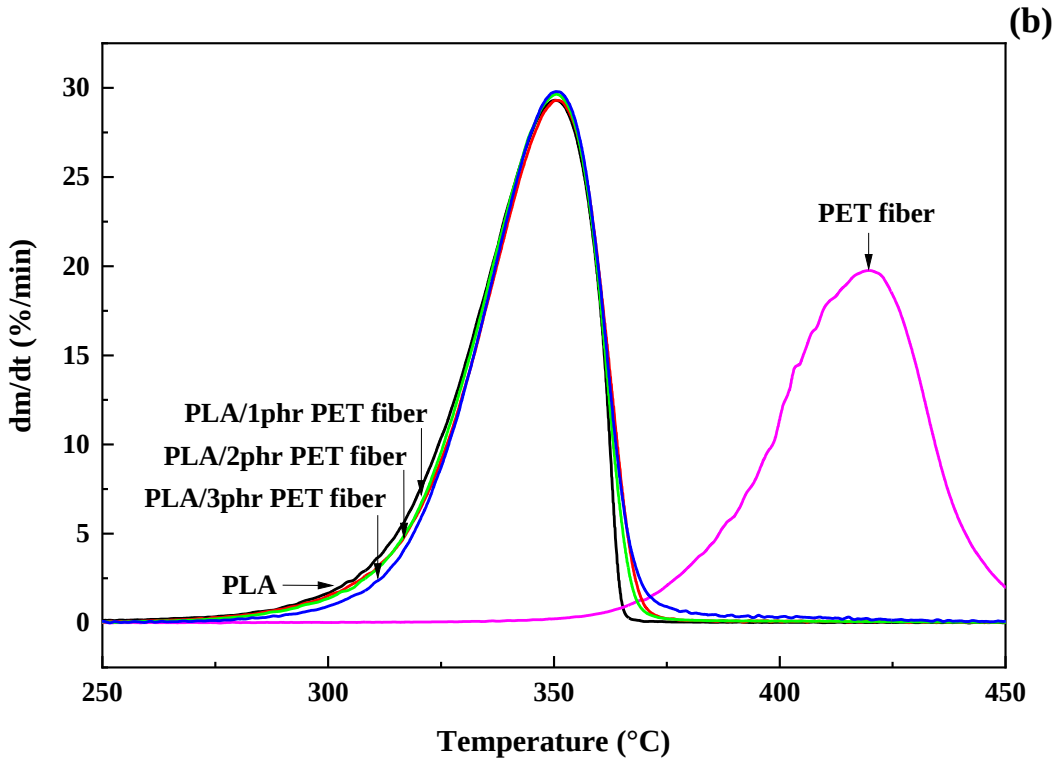
(b)
dm/dt (%/min)
Temperature (°C)
PET fiber
PLA/1phr PET fiber
PLA/2phr PET fiber
PLA/3phr PET fiber
PLA

Figure 9(b).

764 **Figure captions**

Figure 1. Variation of the mixing torque versus time for neat PLA and PLA/PET fiber composites.

Figure 2. Variation of **(a)** the storage modulus and **(b)** tan δ as a function of temperature for neat PLA and PLA/PET fiber composites.

Figure 3. Variation of Izod impact strength for neat PLA and PLA/PET fiber composites as a function of the PET fiber loading. The dotted line corresponds to Izod impact strength of the neat PLA.

Figure 4. SEM micrographs of **(a)** neat PLA, **(b)** PET fiber, and PLA/PET fiber composites: **(c)** PLA/0.5phr PET fiber, **(d)** PLA/2phr PET fiber, and **(e)** PLA/3phr PET fiber.

Figure 5. ATR-FTIR spectra of PLA, PET fiber and PLA/PET fiber composites.

Figure 6. Schematic representation of the physical interactions between the PLA matrix and the PET fiber.

Figure 7. DSC curves of neat PLA, PET fiber, and PLA/PET fiber composites: **(a)** first heating run, **(b)** cooling run, and **(c)** second heating run.

Figure 8. XRD patterns of neat PLA, PET fiber and PLA/PET fiber composites.

Figure 9. **(a)** TGA and **(b)** DTGA curves of neat PLA, PET fiber and PLA/PET fiber composites.

765